J Neurooncol (2009) 94:1–19
DOI 10.1007/s11060-009-9919-z

PRIORITY REPORT

Molecular properties of CD133+ glioblastoma stem cells derived from treatment-refractory recurrent brain tumors

Qinghai Liu · David H. Nguyen · Qinghua Dong · Peter Shitaku · Kenneth Chung · On Ying Liu · Jonathan L. Tso · Jason Y. Liu · Veerauo Konkankit · Timothy F. Cloughesy · Paul S. Mischel · Timothy F. Lane · Linda M. Liau · Stanley F. Nelson · Cho-Lea Tso

Received: 13 February 2009 / Accepted: 5 May 2009 / Published online: 26 May 2009

Abstract Glioblastoma multiforme (GBM) remains refractory to conventional therapy. CD133+ GBM cells have been recently isolated and characterized as chemo-/radio-resistant tumor-initiating cells and are hypothesized to be responsible for post-treatment recurrence. In order to explore the molecular properties of tumorigenic CD133+ GBM cells that resist treatment, we isolated CD133+ GBM cells from tumors that are recurrent and have previously received chemo-/radio-therapy. We found that the purified CD133+ GBM cells sorted from the CD133+ GBM spheres express SOX2 and CD44 and are capable of clonal self-renewal and dividing to produce fast-growing CD133− progeny, which form the major cell population within GBM spheres. Intracranial injection of purified CD133+, not CD133− GBM daughter cells, can lead to the development of YKL-40+ infiltrating tumors that display hypervascularity and pseudopalisading necrosis-like features in mouse brain. The molecular profile of purified CD133+ GBM cells revealed characteristics of neuroectoderm-like cells, expressing both radial glial and neural crest cell developmental genes, and portraying a slow-growing, non-differentiated, polarized/migratory, astrogliogenic, and chondrogenic phenotype. These data suggest that at least a subset of treated and recurrent GBM tumors may be seeded by CD133+ GBM cells with neural and mesenchymal properties. The data also imply that CD133+ GBM cells may be clinically indolent/quiescent prior to undergoing proliferative cell division (PCD) to produce CD133− GBM effector progeny. Identifying intrinsic and

Electronic supplementary material The online version of this article (doi:10.1007/s11060-009-9919-z) contains supplementary material, which is available to authorized users.

Q. Liu · D. H. Nguyen · Q. Dong · K. Chung · O. Y. Liu · J. L. Tso · C.-L. Tso (✉)
Department of Medicine, Division of Hematology-Oncology, David Geffen School of Medicine, University of California Los Angeles, Factor Building, Rm 13-260, 10833 Le Conte Avenue, Los Angeles, CA 90095, USA
e-mail: ctso@mednet.ucla.edu

P. Shitaku · P. S. Mischel
Department of Pathology and Laboratory Medicine, David Geffen School of Medicine, University of California Los Angeles, Los Angeles, CA, USA

J. Y. Liu · S. F. Nelson
Department of Human Genetics, David Geffen School of Medicine, University of California Los Angeles, Los Angeles, CA, USA

V. Konkankit · L. M. Liau
Department of Neurosurgery, David Geffen School of Medicine, University of California Los Angeles, Los Angeles, CA, USA

T. F. Cloughesy
Department of Neurology, David Geffen School of Medicine, University of California Los Angeles, Los Angeles, CA, USA

T. F. Lane
Department of Ob-Gyn and Biological Chemistry, David Geffen School of Medicine, University of California Los Angeles, Los Angeles, CA, USA

T. F. Cloughesy · P. S. Mischel · T. F. Lane · L. M. Liau · S. F. Nelson · C.-L. Tso
Jonsson Comprehensive Cancer Center, University of California Los Angeles, Los Angeles, CA, USA

extrinsic cues, which promote CD133+ GBM cell self-renewal and PCD to support ongoing tumor regeneration may highlight novel therapeutic strategies to greatly diminish the recurrence rate of GBM.

Keywords Glioblastoma · Cancer stem cells · Self-renewal · Radial glial cells · Neural crest cells · Expression microarray

Introduction

Glioblastoma multiforme (GBM, World Health Organization/WHO grade IV) remains virtually incurable despite extensive surgical excision and post-operative adjuvant radio/chemotherapy. Currently, most anti-cancer therapies aim to eliminate rapidly proliferating tumor cells; thus, the novel discovery of rare and radioresistant CD133+ GBM stem cells possessing the enhanced ability to repopulate tumors by multiple laboratories [1–5] provide a potential model to explain the inability to eradicate malignant GBM tumors. Tumor recurrence after treatment may mimic the scenario of post-injury tissue repair and regeneration. Many adult tissues undergo renewal after aging or injury, and hence require a new supply of cells originating from specialized tissue stem cells with the capability to undergo self-renewal, asymmetric cell division, and multipotent differentiation to repair aged cells or damaged tissue [6–9]. Stem cells often reside in stem cell niches that provide a specialized environment to maintain and regulate their properties and activity [10, 11]. The cellular hierarchy of tissue regeneration by resident stem cells has been described in the hematopoietic system, gut, and skin [12–14]. Tissue stem cells are most often slow-cycling and give rise to daughter transient amplifying cells (TAC) that make up the majority of the proliferative cell population in the tissues, and eventually differentiate into non-proliferative cells of a particular tissue type [15, 16]. The studies of airway injury/repair in animal model indicated that airway stem cells will only be induced to self-renewal when an abundant number of TAC are depleted [17, 18], and the elimination of the progenitor and stem cell pools has a consequent failure of tissue regeneration [19]. Thus, at the functional level, CD133+ GBM stem cells behave in ways that are similar to tissue stem cells; CD133+ GBM stem cells can self-renew and reconstitute the original tumor tissue when grafted into mice [1–5]. Cancer stem cells possess a multi-lineage differentiation capacity support for the hypothesis that cancer hierarchy is a result of developmental diversity among cancer cells in different states of differentiation [20–22]. However, it is plausible that multiple genetic and/or epigenetic instability that take place within tumor stem cells might prevent progeny from undergoing non-proliferative terminal differentiation, leading to uncontrolled tumor growth [23–25].

To access genes and pathways potentially associated with malignant features of GBM tumors, we recently compared the genome-wide transcription profile of GBM tumors with that of normal brain tissue and lower-grade astrocytoma [26–28]. Besides those genes associated with inflammation, coagulation, angiogenesis, and tissue remodeling, a series of genes linked with neural stem cell (NSC), mesenchymal stem cells (MSC) and skeletal/cartilage development, was determined. It thus implicates that a tissue regeneration-like reaction is constitutively activated within GBM tumor situ. The molecular profiles of tumor samples obviously do not reflect those of the CD133+ cancer stem cell population, which only forms a small fraction of the whole tumor tissue samples. In this study, we characterized CD133+ GBM stem cells purified from the passaged CD133+ GBM sphere cultures established from recurrent GBM tumors that had previous treatment. Our results indicated that these CD133+ GBM cells have an unlimited ability to repopulate tumor spheres in cultures and are capable of reconstituting a tumor in mouse brain that displays the key histopathologic features of malignant GBM tumor. Molecular profile analysis revealed CD133+ GBM cells possess neuroectodermal-like cell properties endowed with mesenchymal differentiation and astrogliogenic potentials. Additionally, a list of over-expressed genes characterized a quiescent-like state, implying that CD133+ GBM stem cells may be clinically indolent prior to entering the proliferative phase of the cell cycle to attain their malignant phenotype [29].

Materials and methods

Culture of primary GBM cells and tumor spheres

The tumor specimens were obtained from patients who underwent surgery at University of California at Los Angeles (UCLA) Medical Center. All samples were collected under protocols approved by the UCLA Institutional Review Board. The histopathologic typing and tumor grading were done by one neuropathologist according to the WHO criteria. Tumors were enzyme-digested and washed, followed by red blood cell lysis of the pellet. Cells were cultured in a serum-free NSC medium containing DMEM/Ham's F-12 (Mediatech, Manassas, VA) supplemented with 20 ng/ml human recombinant epidermal growth factor (EGF, Sigma-Aldrich, St. Louis, MO), 20 ng/ml basic fibroblast growth factor (FGF, Chemicon, Billerica, MA), 10 ng/ml leukemia inhibitory factor (LIF, Chemicon), and 1× B27 without vitamin A (Invitrogen, Carlsbad, CA). In some cases, cells were cultured in DMEM/Ham's F-12 supplemented with 5% fetal bovine serum for 1–2 passage

followed by switching into NSC culture condition as previously reported [4]. The D431 spheres were derived from a patient with primary/de novo GBM and S496 spheres were derived from a patient with secondary/progressive GBM [27]. Both tumors received radiation and chemotherapy prior to their recurrence and re-operation. GBM sphere cultures were split with acutase weekly (Sigma-Aldrich, St. Louis, MO) and replaced with fresh media every other day.

Real-time quantitative (qt) and semi-qt reverse transcriptase polymerase chain reaction (RT-PCR) analysis

Real-time qtRT-PCR and semi-qtRT-PCR analysis were performed to verify the expression of selected genes in CD133+ GBM cells and patient tumors. Samples were subjected to total RNA extraction with RNeasy kit (QIAGEN, Valencia, CA) and reverse transcription by using a Taqman RT Reagent Kit (Applied Biosystems, Foster City, CA). Two microgram of purified total RNA was used *as* template in RT and cDNA synthesis was done for 1 cycle at 50°C for 30 min and 94°C for 2 min. Real-time qtRT-PCR was carried out with MJ Opticon PCR Analyzer (MJ Research, Inc., Waltham, MA) using SYBR Green PCR Core Reagents (Applied Biosystems). The reactions were cycled 30 times [50°C for 2 min and 95°C for 10 min (94°C for 15 s, 58–60°C for 1 min, and 72°C for 1 min) × 30 cycles] and the fluorescence was measured at the end of each cycle to construct amplification curves. A melting curve was done to verify the specificity of PCR products. Quantitation of transcripts was calculated based on a titrated standard curve co-run in the same experiment and calibrated with the expression level of housekeeping gene (β-actin). The semi-quantitative RT-PCR analysis was performed, using 5 µl cDNA equivalents to 100 ng total RNA. The PCR reaction cycles were carried out as described above. After amplification, PCR products (5 µl) were electrophoresed on 2% agarose gel and visualized under ultraviolet light after SYBR Green staining. Primer 3 Input (http://frodo.wi.mit.edu/cgi-bin/primer3/primer3_www.cgi) was used to selected primers and nonredundant specific primer sequences was verified using National Center for Biotechnology Information BLAST (http://www.ncbi.nlm.nih.gov/blast/Blast.cgi). The primer sequences and expected size of amplified PCR products are listed at supplementary Table 8.

Cell proliferation assay

The proliferative activity of pre-sorted and post-sorted CD133+ and CD133− GBM cells was determined by 3-(4,5-dimethylthiazol-2-yl)-5-(3-carboxymethoxyphenyl)-2-(4-sulfophenyl)-2H-tetrazolium (MTS/PMS) colorimetric assay (Promega, Madison, WI) according to the manufacturer's instructions. Cells were seeded into 96-well tissue culture plates at a density of 10,000 cells per well in triplicate in NSC selecting media and incubated for 24 h. The optical density was measured at 490 nm after 4-h incubation with MTS/PMS reagent.

Loss of heterozygosity analysis

Genomic DNA from sorted CD133+ GBM cells was amplified, labeled, and hybridized under the manufacturer's recommended conditions using the GeneChip Human Mapping 10 K Array *Xba*I 131 (Affymetrix, Santa Clara, CA). Raw allele scores were processed using Affymetrix GeneChip Chromosome Copy Number Tool 1.1 to estimate genome-wide chromosomal gains and losses.

Animal studies and preparation of paraffin slides and frozen sections

Tumorigenicity of GBM cells was determined by injecting the cells orthotopically. Six-week-old female or male Beige/SCID mice were anesthetized and positioned into a stereotactic frame. A burr hole was made using a Dremel drill approximately 3 mm lateral and 1 mm posterior to the intersection of the coronal and sagittal sutures (bregma). Cells were injected using a Hamilton syringe at a depth of 3 mm in a volume of 2 µl. Animals were sacrificed when any sign of neurological symptoms and morbidity/moribundity was observed. Brain tissue were immediately removed and fixed in 10% formalin for 24 h and then transferred to 70% ethanol. Mouse brains were embedded in paraffin in an automatic tissue processor. Brains were sectioned at 5-µm thickness and were mounted on microscope slides. Brain tissue for frozen sections was placed in O.C.T. embedding medium (Tissue-Tekm, Miles Inc.). The sample tray was briefly dipped in liquid nitrogen and was sectioned at 5-µm thickness in a −20°C cryostat and air-dried. Slides were then stored at −70°C until used for hematoxylin and eosin (H–E) stain and immunohistochemical analysis.

Immunocytochemical, histopathological, and immunohistochemical analysis

The immunocytochemical analysis was performed on GBM spheres seeded on an eight-chamber culture slide in the presence of FGF/EGF/LIF for 48 h. Cells were washed, fixed in 4% paraformaldehyde and subjected to immunofluorescent staining. The following primary antibodies were used: CD133 (1:100, Abcam, Cambridge, MA), nestin (1:200, Chemicon, Temecula, CA), SOX2 (1:400; R&D System, Minneapolis, MN), CD105 (3 µg/ml, R&D System), YKL-40 (1:50, Quidel, San Diego, CA) and collagen

type I (1:50, Santa Cruz Biotech, Santa Cruz, CA). After washing, cells were incubated with rhodamine red or Alexa Fluor 488-conjugated goat anti-mouse IgG or goat anti rabbit IgG (1:200, Invitrogen) and counterstained with Hoechst 33342 (Invitrogen) to identify all nuclei. Histopathological analyses were performed on frozen section or paraffin slides stained with H–E staining as per standard technique. Immunohistochemical staining was performed on frozen-section slides. Slides were subject to a 1-h blocking step followed by the application of primary antibody or control antibody for 1 h at room temperature. The following primary antibodies were used: CD31 (1:100, Biocare Medical, Concord, CA), CD133, YKL-40 (1:100), and SOX2 (1:100). The immunodetection was performed using Vectastain ABC Standard kit and Vector NovaRED (Vector Laboratories, Burlingame, CA).

Fluorescence-activated cell sorting analyses and purification of CD133+ GBM cells

Fluorescence-activated cell sorting analyses (FACS) analyses were employed to determine the percentage of cells expressing stem cell markers. Dissociated cells were stained with the following antibodies for 30 min at 4°C: anti-CD133-APC (Miltenyi Biotech, Auburn, CA), anti-CD44-FITC (Caltag Laboratories, Burlingame, CA), anti SOX2 (indirect staining, using Alexa Fluor 488-conjugated goat anti-mouse IgG) and fluorescence-conjugated isotype IgG controls. 10,000 events were collected in each analysis. The analyses were performed on a FACSCalibur flow cytometer (Becton Dickinson, San Jose, CA) and ≥10,000 events were collected in each analysis. To purify CD133+ GBM cells, dissociated cells were immunostained with anti-CD133-APC under the sterile condition. The CD133+ and CD133− cells were sorted and collected on a BD FACSAria^{TM} II cell sorter at 70 psi using a 70-μm nozzle. The purity of post-sorted cells was determined.

Microarray procedures and data analysis

Molecular profiling and analysis were performed as described [27]. Briefly, cDNA was generated and converted to cRNA probes using standard Affymetrix protocols and hybridized to Affymetrix GeneChip U133 Plus 2.0 Array. The chips were scanned using the GeneArray scanner (Affymetrix). The CEL files generated by the Affymetrix Microarray Suite version 5.0 were converted into DCP files using the DNA-Chip Analyzer (dChip 1.3; http://biosun1.harvard.edu/complab/dchip/). The DCP files were globally normalized, and gene expression values were generated using the dChip implementation of perfect-match minus mismatch model-based expression index. To avoid inclusion of low-level and unreliable signals, the higher signal needed to exceed 100 and be called present by MAS 5.0 in >30% of the samples. All group comparisons were performed in dChip.

Gene annotation

Functional annotation of individual gene was obtained from NCBI/Entrez Gene (http://www.ncbi.nlm.nih.gov/sites/entrez), the published literature in PubMed Central (NCBI/PubMed), Online Mendelian Inheritance in Man (NCBI/OMIM), Source database (http://source.stanford.edu/cgi-bin/source/sourceSearch), Protein knowledgebase (UniProtKB) (http://beta.uniprot.org/), and Information Hyperlinked over Proteins (http://www.ihop-net.org/UniPub/iHOP/). Functional categorization of expression-based clusters based on gene ontology (GO) was performed using a web tool dChip v1.3 software (http://www.hsph.harvard.edu/~cli/complab/dchip/). After the hierarchical clustering was performed on genes, dChip searches all branches with at least four functionally annotated genes to assess whether a local cluster is enriched by genes having a particular function with GO term.

Results

GBM spheres contain a minor population of CD133+ cells and express neural and mesenchymal stem cell-associated markers

Five GBM sphere cultures were initiated under NSC-selective culture conditions; two of them (D431 and S496) were expandable, and were used for current study. GBM spheres were dissociated, clonally replated to prevent cells from forming aggregates (4×10^4 cells/7 ml/10 cm dish), and passaged weekly. Most notably, individual cells dissociated from spheres showed distinct proliferative potentials; some form abortive colonies, whereas others form larger colonies varying in size (Fig. 1A), suggesting that cells which formed spheres, are heterogeneous. When compared to autologous GBM cell cultures growing in serum-containing media, a more differentiated state, in which a negligible percent of cells express CD133 (<0.5%), 7–10% CD133+ GBM cells could be detected in GBM sphere cultures, using FACS analysis (Fig. 1B). Moreover, sphere formation analysis by limiting dilution assay revealed 7–15% clonogenic efficiency (Fig. 1C), indicating that the majority of cells within spheres are not sphere-reinitiating cells. We then test whether these bulk CD133+ GBM spheres that contain majority of CD133− GBM cells express GBM tumor-associated genes that are linked with NSC and MSC and their cell lineages as identified in GBM tumors [26–28]. Indeed,

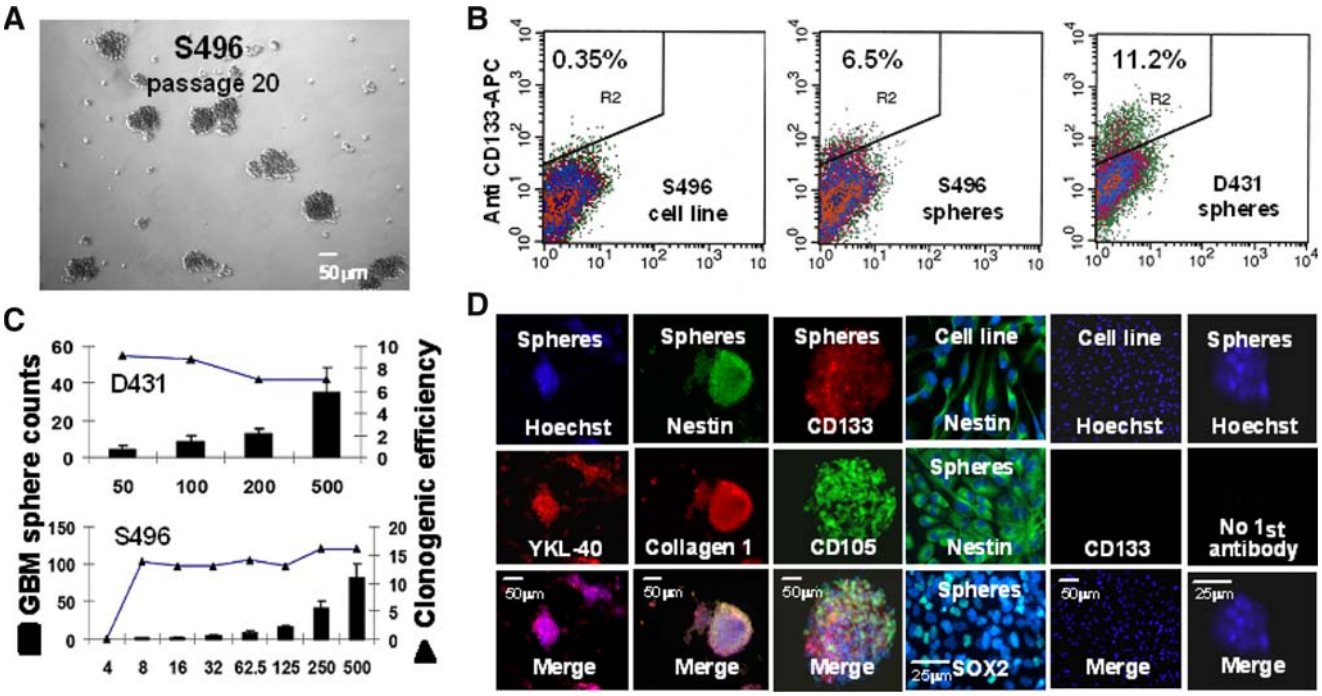

Fig. 1 CD133+ glioblastoma (GBM) sphere culture derived from treated and recurrence GBM tumors express neural and mesenchymal stem cell-associated genes. **A** Under neural stem cell (NSC)-selective conditions, passaged and dissociated GBM spheres can generate single cells, small spheres, and large spheres (>50 cells), indicating tumor spheres consist of progeny with different proliferative potentials. Scale bar = 50 μm. **B** Propagated GBM sphere cultures contain ~7% to 10% of the CD133+ GBM cells determined by flow cytometry analysis. **C** The clonogenic efficiency of dissociated CD133+ GBM spheres assayed by the limiting dilutions relatively correlates to the % of the CD133+ cells determined in the GBM spheres. **D** CD133+ GBM spheres express neural and mesenchymal/chondrogenic-associated genes as indicated, determined by immunocytochemical analysis. Scale bar = 25 or 50 μm, as indicated

immunostaining analysis revealed several NSC- and MSC-associated markers, including SRY (sex-determining region Y)-box 2 (SOX2), nestin, YKL-40, collagen Type I, and CD105 (endoglin) were determined (Fig. 1D). RT-PCR analysis was used to confirm the expression of additional GBM markers, including maternal embryonic leucine zipper kinase (MELK), platelet-derived growth factor receptor-alpha (PDGFR-a), SOX4, and musashi homolog 1 (MSI1) (data not shown), demonstrating that cultured CD133+ GBM spheres express molecular markers of stem-like GBM tumors.

CD133+ GBM spheres were generated and maintained by CD133+ GBM cells through self-renewal and proliferative cell division

To determine whether CD133+ GBM cells are sphere-re-initiating cells, and responsible for generating CD133− GBM progeny within spheres, CD133+ GBM cells were sorted from dissociated CD133+ sphere cultures using specific CD133 antibody and FACS analysis (Fig. 2A). The purity of post sorted CD133+ cells ranged from 92% to 97%. Purified CD133+ cells were seeded in 96-well plates at the clonal density by limiting dilution. Notably, daughter cells divided from a single CD133+ GBM cell grow rapidly and gradually pile up to form GBM spheres. Moreover, populated cells are morphologically heterogeneous revealed by differences in cell size and the formed spheres showed variation in shape (Fig. 2B) [30]. These proliferative dividing cells are mostly CD133− cells as evident by the determination of ~90% CD133− GBM cells in the expanded spheres (Fig. 2C). Meanwhile, ~10% CD133+ GBM cells were determined in single cell-initiated spheres, indicating CD133+ GBM cells could clonally self-renew, but apparently be maintained in a slow-dividing status distinct from CD133− progeny. RT-PCR analysis also provided evidence for the presence of proliferative CD133− daughter cells within the growing spheres, which showed a decreased level of CD133 transcripts compared to that of purified CD133+ GBM cells (Fig. 2D). These data thus demonstrate that CD133+ GBM cells are capable of clonal self-renewal and giving rise to fast-growing CD133− daughter cells.

To test whether CD133+ cells are responsible for the continuous propagation of GBM sphere in cultures, we compared the growth expansion of purified CD133+ cell-initiated cultures with that of cultures initiated by the purified CD133− progeny (Fig. 2E). In order to ensure that CD133+ cells were completely removed from the CD133− fraction, post-sorted CD133− cells were

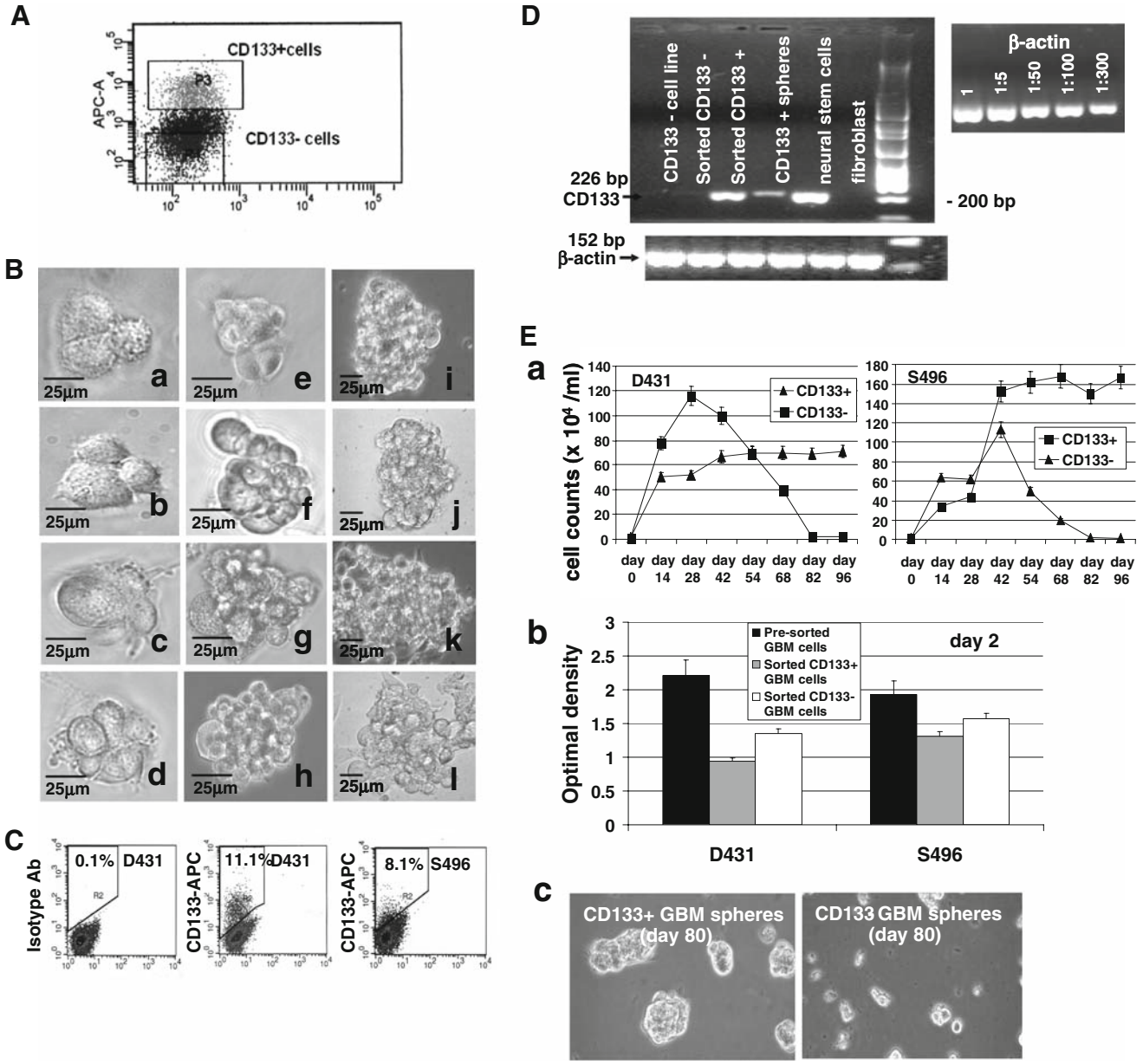

Fig. 2 CD133+ GBM cells are sphere-reinitiating cells capable of undergoing clonal self-renewing and proliferative cell division in order to repopulate spheres. **A** Purification of CD133+ GBM cells from bulk CD133+ sphere cultures using specific anti-CD133 antibody and fluorescence-activated cell sorter. **B** A single CD133+ GBM cell can undergo proliferative cell division to generate daughter cells that are morphologically heterogeneous as revealed by cell size. Scale bar = 25 μm. **C** GBM spheres initiated by a single CD133+ GBM cell contain ~10% CD133+ GBM cells as determined by flow cytometry analysis. **D** RT-PCR analysis showed that purified CD133+ GBM cells overexpress CD133 transcripts compared with GBM spheres. Sorted CD133− GBM cells, serum-cultured GBM cell lines, and fibroblasts do not express CD133 transcripts. Normal neural stem cells served as positive control cells, show a strong signal for CD133. Beta-actin was served as an internal loading control. **E** The growth expansion assays indicated that GBM sphere cultures initiated by CD133+ GBM daughter cells, not CD133− GBM daughter cells, can be propagated for indefinite passages. (*a*) Cells were seeded in 6-well plates at a cell density of 10^4 cells per well in triplicates. Cells were counted approximately every 2 weeks and reseeded at the same cell density. (*b*) Short-term proliferation assay performed in day 2 cultures indicated that freshly sorted CD133+ GBM cells exhibited less proliferative activity compared to the that of CD133− GBM cells sorted from the same sphere culture, as determined by MTS/PMS colorimetric assay. Bars represent the mean ± standard error of triplicate wells. (*c*) CD133+ GBM cells, not CD133− GBM cells, sorted from the same CD133+ GBM sphere cultures can repopulate GBM spheres for indefinite passages

subjected to a second round of cell sorting. The purified CD133+ and CD133− daughter cells sorted from the same CD133+ GBM sphere cultures initiated by the CD133+ GBM cells were respectively seeded in triplicate in 6-well plates at the cell density of 10^4 cells/2 ml/well. Cell counting was performed biweekly. Most notably, the

growth initiation of cell cultures seeded by purified CD133+ GBM cells (40–50 × 10^4 cells/ml in first cell counting) was delayed compared to that of purified CD133− GBM cell-seeded culture (70–80 × 10^4 cells/ml), which showed an enhanced growth rate in the early passages (Fig. 2E, a). This determination was verified by a short-term (24 h) proliferation assay on day 2 after sorting, which also indicated a slower growth rate of freshly purified CD133+ GBM daughter cells compared to CD133− GBM daughter cells sorted from the same sphere cultures (Fig. 2E, b). We however, observed a lesser difference in proliferative activity between CD133+ S496− and CD133− S496 cell-seeded cultures compared to the growth differences between CD133+ and CD133− D431 cell-seed cultures. This may be due to purified CD133+ S496 GBM cell culture being able to drop from ≥95% purity to 5–10% within ∼3 to 5 days, whereas it will take ∼2 weeks to drop to ∼10% to 15% in D431 cells (data not shown). Nevertheless, the pre-sorted GBM cells from the dissociated CD133+ GBM spheres showed a better proliferative activity than sorted CD133+ or CD133− cells in either cases (Fig. 2E, b). The growth of CD133− GBM cell-initiated cultures gradually dropped after repeated passaging in contrast to that of CD133+ cell-initiating cultures, which showed a stable expansion (Fig. 2E, a, c). These results thus indicate that CD133+ GBM cells have the capacity for unlimited self-renewal, which is required for a long-term propagation of D431 and S496 GBM spheres in cultures.

Cells spontaneously migrate out of GBM spheres and form the surrounding monolayer

It was reported that neural precursor cells migrating out of neurospheres in cultures and outgrowing into a monolayer [31, 32]. We have also observed a similar in vitro characteristic in GBM sphere cultures. GBM cells can spontaneously migrate radially outward from the semi-adherent and flattened GBM sphere bodies, resulting in a rim of monolayer cells surrounding the spheres (Fig. 3A, a–e). Eventually, these migrating cells outgrow into an adherent monolayer that spread out over the surface of the culture dish (Fig. 3A, f). Unexpectedly, these cultures contain a higher percentage of CD133+ GBM cells (15–30% for S496 and 50–70% for D431) than non-adherent sphere cultures (Fig. 3B, a, b). The majority of CD133+ GBM cells co-express SOX2 and CD44 (Fig. 3B, c, d) as those of CD133− progeny in same cultures, indicating that CD133+ GBM cells sharing some of their surface markers with their immediate progeny grew in the same cultures. Since no additional factors were added into the culture to influence the behavior of cells, such a cell migration may be an intrinsic property that reflects inherently migratory properties of the GBM tumor of origin, which may confer a infiltrative nature of GBM tumors in brain that is characterized by the ability to migrate and invade the adjacent healthy brain tissue. When these adherent cells were dissociated and replated at clonal density, they can regrow as sphere cultures (Fig. 3B, e) containing ∼10% CD133+ cells (Fig. 3B, f).

CD133+ GBM cells exhibit genomic abnormalities and are capable of repopulating malignant GBM tumor in mouse brain

Both CD133+ D431 GBM cells and CD133+ S496 GBM cells exhibited loss of heterozygosity (LOH) at various chromosome locations as determined using a high-density single nucleotide polymorphism array analysis. Particularly, LOH at chromosome 10 was found in both CD133+ GBM cells, whereas only CD133+ S496 GBM cells exhibited LOH in chromosome 17 (Fig. 3C). Additionally, chromosome 7 was found to be amplified in CD133+ D431 GBM cells, and to a lesser degree in S496 cells. Similar results were found in the autologous cell line cultures passaging in the serum-containing media [28]. To compare the in vivo fate of CD133+ GBM cells and CD133− GBM cells, cells were stereotactically injected into the brains of SCID mice. Mice that received purified CD133+ GBM cells (5–10 × 10^3/2 μl) (11/12) sorted from the CD133+ GBM sphere cultures (6 mice per cell type) showed impaired mobility at week 15–28 post-injection, whereas mice that received CD133− GBM cells (5 × 10^5/2 μl) (0/20) (10 mice per cell type) remained normal at week 30. The injected CD133− GBM cells include CD133− GBM cells sorted from the same CD133+ GBM sphere cultures that were used for sorting CD133+ GBM cells (post two rounds of cell sorting) (0/6), the CD133− cells sorted from autologous GBM cell line cultured in serum (0/6) (note, serum-cultured GBM cells contain 0.2–0.35% CD133+ cells) and serum-cultured GBM cells switched to NSC culture media for 48 h (0/4) and 6 days (0/4). The H–E staining of tumors demonstrated hypercellular zones surrounding necrotic foci that form the histopathologic features of pseudopalisading necrosis as seen in human glioblastoma (Fig. 3D). Notably, S496 tumors (Fig. 3D, a–e) exhibited more enhanced necrosis than that of D431 tumors (Fig. 3D, f–i). Immunohistochemical staining revealed hypervascularity evidenced by the strong expression of CD31/platelet endothelial cell adhesion molecule-1 (PECAM-1) (Fig. 3D, k, l). The CD133 immunoreactive cells were occasionally found (Fig. 3D, m, n), suggesting the CD133− GBM daughter cells play the key role in promoting the malignant features of tumor in mice. The expression of nestin, SOX2, and YKL-40 in infiltrating tumor cells (Fig. 3D, o–q) verified the GBM origin and tumorigenic potential of CD133+ GBM cells.

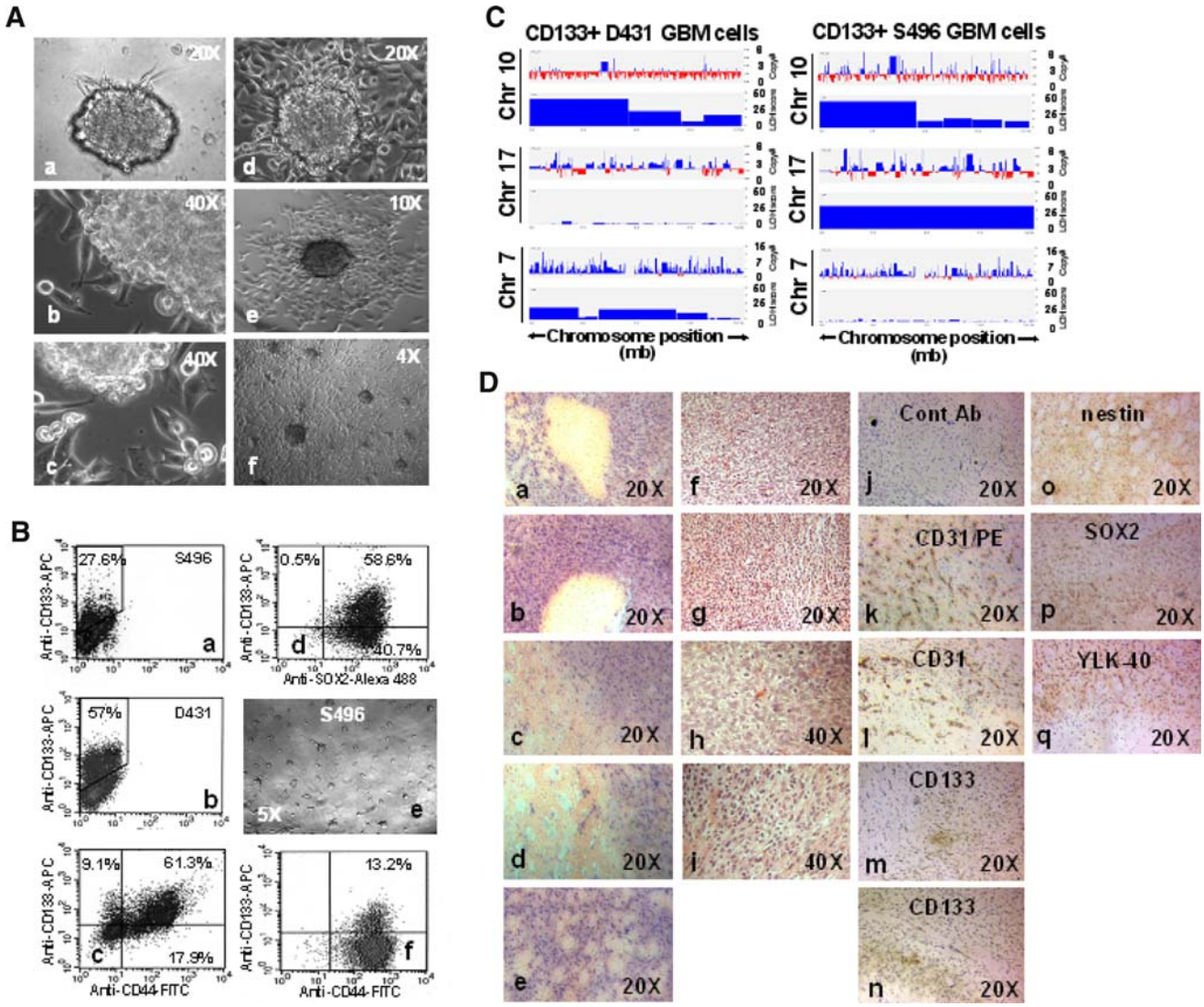

Fig. 3 CD133+ GBM cells can reconstitute an infiltrating GBM tumor in mouse brain that displays hypervascularity and pseudopalisading necrosis-like features. **A** Passaged CD133+ GBM spheres (>20 passage) can radially migrate out of spheres extensively (*a–f*). Magnification, 40× (*f*), 100× (*e*), 200× (*a*, *d*), 400× (*b*, *c*). **B** The flow cytometry analysis indicated that the adherent GBM sphere cultures contain a higher percentage of CD133+ cells (20–70%) that coexpressed SOX2 and CD44 (*a–d*). Replating adherent CD133+ GBM sphere culture cells at clonal cell density can re-initiate spheres that contain ~10% CD133+ GBM cells (*e*, *f*). **C** Genomic abnormalities that are associated with glioblastoma were detected in CD133+ GBM cells. CD133+ GBM cells were evaluated for allelic imbalances and chromosomal copy number abnormalities by using a high-density single nucleotide polymorphism array analysis. *X* axis, length of chromosomes 17, 10, and 7; *Y* axis, score of the evidence of LOH or gain of gene copy. **D** Intracranial injection of purified CD133+, not CD133− GBM daughter cells, can lead to the development of infiltrating tumors. HE staining shows hypercellular zones surrounding necrotic foci and the formation of a clear space (*a–i*). The hypervascularity was displayed by the strong positivity of CD31/PECAM-1 (platelet endothelial cell adhesion molecule-1) as determined by immunostaining (*k*, *l*). CD133 immunoreactive cells were occasionally found in small clusters (*m*, *n*). The expression of nestin, SOX2, and YKL-40 in the infiltrating cells validates the origin of human malignant GBM tumor (*o–q*). No immunoreactivity was determined when the control antibody was applied (*j*). Magnification, 200× (*a–g*; *j–q*), 400× (*h*, *i*)

Shared CD133+ GBM cell-associated genes revealed neuroectodermal properties and a quiescent/antiproliferative phenotype

To explore molecular properties of CD133+ GBM cells, we performed large-scale gene expression analysis using DNA microarrays. Based on the in vitro characterization, it is anticipated that CD133+ and CD133− daughter cells sorted from the same CD133+ sphere cultures initiated by CD133+ GBM cells will share certain properties (e.g. CD44, nestin, SOX2). Therefore, to assess genes that characterized the tumorigenic, stem-like CD133+ GBM

cells, we first compared the mean level of normalized expression profiles in each of the two purified CD133+ GBM cell samples (D431 and S496) ($n = 3$ preparations, passage 20, 29, 40) against the non-tumorigenic, autologous CD133− GBM cells growing in serum (more differentiated condition) with and without switching to a short-term NSC culture condition (24 h, 48 h, and 6 days) ($n = 6$ preparations). The short-term culture of cells in NSC culture condition diminishes the likelihood of identifying NSC growth factor-responsive genes (background genes) in the comparative analysis. Probe set signals on the expression array that were ≥3-fold higher in each CD133+ GBM cell group versus the autologous CD133− GBM cell group with a pairwise *t*-test ($P < 0.05$) were selected. The filtering criteria were described in Materials and Methods. Sixty-four shared genes overexpressed in CD133+ GBM cells were identified in both pairwise comparisons (D431 and S496), and CD133/prominin1 was highly differentially expressed (D431 = 53 folds, S496 = 14 folds) as anticipated, which validates a good purification process (Table 1; Fig. 4A, a). The distinctive gene expression profiles of selected genes were verified by real-time qt-RT-PCR and semi-qt-RT-PCR (supplementary Fig. 1). The gene function enrichment analysis identified 24 significant GO clusters (Fig. 4A), and 38% (find 24 genes), 25% (find 17 genes) and 25% (find 17 genes) genes were found for GO terms related to "development" ($P = 0.000001$), "system development" ($P = 0.000000$) and "nervous system development" ($P = 0.000000$)), respectively (supplementary Table 1). Indeed, a large percentage of genes are neuroectoderm-developmental genes (Table 1). Most notably, Dlx5 and Dlx6 (see gene description in Table 1) are regulators of chondrogenesis of limb [33] and are highly expressed in cranial neural crest. MEOX2, MEST, and FABP4 characterized mesenchymal progenitors, and RARA [34] and Wnt antagonist FRZB [35] are likely to be inducing the signals to suppress the chondrocytic and skeletal progenitor differentiation. Simultaneously, many genes reflective of the normal function of neural crest cells were determined: SEMA6D for cardiac development, CHRNA9 for cochlea hair cell development, PPEF1 for development of cranial ganglion sensory neurons, and SHROOM2 for melanosome biogenesis. Moreover, LGR5, a novel marker gene for adult stem cells was determined [36], indicating CD133+ GBM cells share a property with other tissue stem cells.

Meanwhile, a series of genes functioning in antimitotic/antigrowth effect was identified. For instance, MEOX2 suppresses cell proliferation in a p21-dependent manner [37], SULF1 suppresses peptide growth factor signaling and angiogenesis [38], IL17RD antagonizes FGF-induced cell proliferation [39], and FRZB and VLDL act as negative regulators of the Wnt signaling pathway and angiogenesis [40]. Simultaneously, EDN3, a potent mitogen for early neural crest-derived glial and melanocytic precursors [41], and GAP-43, a crucial component of an effective neural regenerative response [42] were determined, implicating a role for maintaining the basic growth activity of CD133+ GBM cells. Thus, the overall molecular profile characterizes CD133+ GBM cells as having a slow-growing, non-differentiated, self-renewing, chondrogenic, and antidevelopmental phenotype.

Unique CD133+ GBM cell-associated genes may reflect inherently migratory properties of GBM tumor of origin

The 50 most strongly differentially expressed genes only over-expressed in each purified CD133+ GBM cells sorted from the CD133+ GBM spheres were selected (supplementary Tables 2 and 3). Uniquely, fatty acid binding protein 7 (FABP7), a migratory radial glial cell (RGC) gene, was identified as the top distinct gene in CD133+ S496. The FABP7 expressing RGC have been proposed to be the malignant glioma cell of origin [43] and the increased expression of nuclear FABP7 was found to be associated with the regions of GBM tumor infiltration, reduced survival, and recurrence [44]. On the other hand, MYCN, a migratory neural crest cell gene, and MDM2, a direct transcriptional target of MYCN, were detected in CD133+ D431. The overexpression of MDM2 is implicated in the development of de novo GBM [45]. Additional genes that are associated with cell migration machinery expressed in either CD133+ D431, CD133+ S496 or both, include genes that are associated with cell polarity (e.g. GPC3, FZD1, EPH receptor B1/B3), motor protein (KIF5C), assembly of microtubules and formation of lamellipodia and filopodia (MAP2, RHOJ, RHOU, TNIK) and formation of actin stress fibers and focal adhesions (SORBS1), pointing to an active migration characteristic of CD133+ GBM cells. More importantly, the determination of Notch effector genes (HEY1, NFIA, ID4, FABP7) reflected the prolonged Notch activation and abrogation of neurogenesis, thereby promoting a migratory phenotype and glial-fate specification [46–50]. In general, both unique gene lists are consistent with "anti-proliferative phenotype" as those of shared genes in Table 1.

CD133− GBM daughter cells divided from CD133+ GBM cells express molecular profiles associated with malignant GBM phenotype

Since CD133+ GBM cells sorted from CD133+ GBM spheres cultures expressed molecular profiles that characterized a quiescent phenotype, it is reasonable to predict that the malignant tumor-associated genes are mainly expressed in CD133− GBM daughter cells, which make up the major

Table 1 Shared genes overexpressed in CD133+ D431 and CD133+ S496 GBM cells compared with autologous CD133− GBM cells cultured in serum-containing media

Gene	Symbol	Gene I.D.	Fold change		Chromosome	Functional involvement
			D431	S496		
Sema, transmembrane, and cytoplasmic domain, 6D	SEMA6D	80031	117.89	4.16	15q21	Guidance of myocardial patterning in cardiac development
Growth associated protein 43	GAP43	2596	110.32	25.56	3q13.1-q13.2	Nervous system regeneration
Distal-less homeo box 6	DLX6	1750	78.94	40.90	7q22	Craniofacial morphogenesis/chondrogenesis
BH-protocadherin (brain–heart)	PCDH7	5099	62.58	3.76	4p15	Calcium-dependent cell–cell adhesion
Prominin 1/CD133	PROM1	8842	52.87	13.70	4p15.32	Neuroepithelial stem cell marker; cell polarity
Endothelin 3	EDN3	1908	43.96	26.35	20q13.2-q13.3	Promotes neural crest cell and precursor proliferation
ST8 alpha-N-acetyl-neuraminide alpha-2,8-sialyltransferase 4	ST8SIA4	7903	43.56	5.39	5q21	Synthesis of polysialic acid in neural stem cells
Transcription factor AP-2 beta	TFAP2B	7021	37.28	23.09	6p12	Neural crest cell growth and differentiation
Distal-less homeo box 5	DLX5	1749	36.64	17.18	7q22	Craniofacial morphogenesis/chondrogenesis
Neurexin 3	NRXN3	9369	27.84	5.79	14q31	Stabilizes synapses
Cholinergic receptor, nicotinic, alpha polypeptide 9	CHRNA9	55584	27.24	3.99	4p14	Cochlea hair cell development
Fatty acid binding protein 4, adipocyte	FABP4	2167	26.43	70.07	8q21	Lipid and glucose metabolism
Peptidase inhibitor 15	PI15	51050	24.09	7.79	8q21.11	Expressed in neuroblastoma/glioblastoma
Cholinergic receptor, nicotinic, alpha polypeptide 1 (muscle)	CHRNA1	1134	23.12	6.33	2q24-q32	Neuromuscular transmission
Glycoprotein M6B	GPM6B	2824	23.12	5.79	Xp22.2	Stabilizes proteolipids in neuron
Sortilin-related VPS10 domain containing receptor 1	SORCS1	114815	19.39	45.42	10q23-q25	Brain neuropeptide receptors
Protein phosphatase, EF-hand calcium binding domain 1	PPEF1	5475	19.18	6.57	Xp22.2-p22.1	Specific sensory neuron function and/or developments
Kinesin family member 5C	KIF5C	3800	19.03	17.36	2q23.1	Neuronal kinesin enriched in motor neurons
Down syndrome critical region gene 1-like 1	RCAN2	10231	18.71	10.06	6p12.3	Suppresses angiogenesis
Leucine-rich repeat-containing G protein-coupled receptor 5	LGR5	8549	18.56	4.59	12q22-q23	Stem cell marker of small intestine, colon, skin, hair
Glutamate receptor, ionotropic, AMPA 1	GRIA1	2890	16.48	14.20	5q31.1	Excitatory neurotransmitter receptors
Mesenchyme homeo box 2	MEOX2	4223	15.64	47.53	7p22.1-p21.3	Somitogenesis; myogenic/sclerotomal differentiation
Monooxygenase, DBH-like 1	MOXD1	26002	15.53	23.19	6q23.1-q23.3	Dopamine-oxygenase; neural crest/ganglia marker
Cholinergic receptor, muscarinic 3	CHRM3	1131	14.44	7.26	1q43	Smooth muscle contraction; secretion of glands
Sulfatase 1	SULF1	23213	13.96	30.43	8q13.2-q13.3	Remove 6-O-sulfate groups of heparan sulfate
Regulator of G-protein signaling 5	RGS5	8490	13.19	15.10	1q23.1	Marker for pericytes; antiangiogenesis
Frizzled-related protein	FRZB	2487	12.98	6.01	2qter	Antagonizes Wnt pathway
Neurocalcin delta	NCALD	83988	11.78	3.54	8q22.2	Neuronal calcium sensors; interact with S100 beta
Gamma-aminobutyric acid (GABA) receptor, rho 1	GABRR1	2569	11.35	5.08	6q13-q16.3	Reduces sensitivity to retinoic acid
Protocadherin 19	PCDH19	57526	11.04	5.16	Xq13.3	Expressed in neuroepithelium
SRY (sex determining region Y)-box 2	SOX2	6657	10.74	7.49	3q26.3-q27	Neural stem cell marker, self-renewal

Table 1 continued

Gene	Symbol	Gene I.D.	Fold change		Chromosome	Functional involvement
			D431	S496		
TRAF2 and NCK interacting kinase	TNIK	23043	9.72	3.41	3q26.2-q26.31	Regulates actin cytoskeleton
Mesoderm specific transcript homolog (mouse)	MEST	4232	8.79	45.13	7q32	Expressed in mesodermal derivatives
Phosphorylase kinase, gamma 2 (testis)	PHKG2	5261	8.79	8.01	16p12.1-p11.2	Activates glycogen phosphorylase
Spondin 1, extracellular matrix protein	SPON1	10418	8.43	33.87	11p15.2	Cementoblastic differentiation; inhibits angiogenesis
Rap guanine nucleotide exchange factor (GEF) 5	RAPGEF5	9771	8.42	19.43	7p15.3See	RAS activator via maintain the GTP-bound state
Trinucleotide repeat containing 9	TOX3	27324	8.36	56.65	16q12.1	Regulation of neurodevelopment or neuroplasticity
Insulin-like growth factor binding protein 2, 36 kDa	IGFBP2	3485	7.83	3.09	2q33-q34	Activation of the Akt and/K-Ras
Death-associated protein kinase 1	DAPK1	1612	7.69	15.44	9q34.1	Tumor suppressor
Formin homology 2 domain containing 3	FHOD3	80206	7.49	3.15	18q12	Present in nestin-expressing neuroepithelial cells
Scrapie responsive protein 1	SCRG1	11341	7.09	80.65	4q31-q32	Mesenchymal chondrogenesis, growth suppression
Potassium large conductance calcium-activated channel	KCNMB4	27345	7.09	6.00	12q	Smooth muscle tone and neuronal excitability
Retinoic acid receptor, alpha	RARA	5914	6.67	12.21	17q21	Marker for prechondrogenic progenitors
Neurofilament, light polypeptide 68 kDa	NEFL	4747	6.6	6.28	8p21	Controls electrical signals travel down the axon
Oxoglutarate (alpha-ketoglutarate) dehydrogenase	OGDH	4967	6.24	4.36	7p14-p13	Krebs cycle
ADAM metallopeptidase domain 23	ADAM23	8745	5.32	4.38	2q33	Tumor suppressor
Cadherin 2, type 1, N-cadherin (neuronal)	CDH2	1000	5.06	11.21	18q11.2	Cell–cell adhesion; left-right asymmetry; cell migration
Immunoglobulin superfamily, member 4C	IGSF4C	199731	4.75	10.07	19q13.31	Tumor suppressor
Ankyrin 3, node of Ranvier (ankyrin G)	ANK3	288	4.71	4.19	10q21	Maintenance of ion channels at nervous systems
Alpha-2-macroglobulin	A2M	2	4.31	11.49	12p13.3-p12.3	Protease inhibitor and cytokine transporter
Inhibin, beta A (activin A, activin AB alpha polypeptide)	INHBA	3624	4.28	7.16	7p15-p13	Tooth development; tumor suppressor
Neuropilin 2	NRP2	8828	4.26	5.98	2q33.3	Axon guidance in the peripheral and central neural system
Very low density lipoprotein receptor	VLDLR	7436	4.18	5.83	9p24	Wnt antagonist; metabolism of apoprotein-E
Sortilin-related VPS10 domain containing receptor 2	SORCS2	57537	3.81	8.95	4p16.1	Brain neuropeptide receptor
GalNAc-T10	GALNT10	55568	3.67	4.30	5q33.2	Predominant expression in CNS
FXYD domain containing ion transport regulator 6	FXYD6	53826	3.49	22.75	11q23.3	Modulator of the Na, K-ATPase
Leucine rich repeat neuronal 3	LRRN3	54674	3.49	3.49	7q31.1	Developing ganglia and motor neurons
Interleukin 17 receptor D	IL17RD	54756	3.44	9.59	3p14.3	Tumor suppressor-like role via FGF signaling
Pleiotrophin	PTN	5764	3.37	4.86	7q33-q34	Heparin binding; neurite growth-promoting factor

Table 1 continued

Gene	Symbol	Gene I.D.	Fold change		Chromosome	Functional involvement
			D431	S496		
Muscleblind-like 2 (Drosophila)	MBNL2	10150	3.15	3.67	13q32.1	Skeletal muscle development
Microtubule-associated protein 2	MAP2	4133	3.09	4.36	2q34-q35	Microtubule assembly in neurogenesis
Apical protein-like (*Xenopus laevis*)	SHROOM2	357	3.06	6.24	Xp22.3	Regulates melanosome biogenesis and localization
EPH receptor B3	EPHB3	2049	3.01	8.71	3q21-qter	Precise guidance of axon and neural crest cell migration
FK506 binding protein 1B, 12.6 kDa	FKBP1B	2281	3.00	4.18	2p23.3	Excitation–contraction coupling in cardiac muscle

Analysis was based on a cutoff of 3-fold increase in relative expression compared to autologous CD133− GBM cells ($P < 0.05$). Individual P value is shown in supplementary Table 7

population of CD133+ GBM spheres and tumors. Indeed, comparative analysis of purified CD133+ and CD133− GBM daughter cells sorted from the same CD133+ GBM sphere cultures that were initiated by the purified CD133+ GBM cells revealed a transition from a tumor suppressive-like profile to tumorigenic profile when CD133+ GBM cells divided and produced CD133− GBM daughter cells. The top 15 genes in molecular changes were presented (Table 2; Fig. 4A, b and c), and the CD133 appears to be the top down-regulated gene in both pairwise comparisons. Uniquely, the gene function category analysis of gene changes in D431 cells identified 5 significant clusters all belong to extracellular component-associated GO terms (Fig. 4A, b), and 10 out of 30 genes (33%) under the GO term "extracellular region"
(P value = 0.000004) (supplementary Table 4). This data thus suggests most genes that are modulated when CD133+ D431 GBM cells undergo cell division and produce fast-growing CD133− D431 daughter cells primarily include genes associated with mesenchymal/extracellular components. Evidently, two top genes, IBSP and YKL-40, determined in CD133− daughter cells are markers of osteoblast/chondrocyte differentiation and are angiogenic factors. More importantly, YKL-40 is linked to the mesenchymal and recurrent GBM phenotype [51]. Several upregulated genes further point to the early onset of inflammatory and angiogenic response. In contrast, genes that are down-regulated in CD133− D431 daughter cells mostly are CD133+ D431 GBM associated genes (anti-proliferative genes) as described (Table 1; supplementary Table 2).

Distinctively, most upregulated genes in sorted CD133− S496 GBM daughter cells are associated with progression of cell cycle (Table 2). The top gene, HMGCS1, is an enzyme involved in the biosynthesis of lipid/cholesterol, a critical component of biological membranes, and is thus upregulated with constant cellular proliferation [52]. Several upregulated genes further point to the early onset of proliferative differentiation, including CEBPZ, a transcription factor for maintaining the cell differentiation state, PIK3C2B, a downstream target of growth factor receptors that link to the activation of the AKT pathway, and PRKACB, a target gene of c-myc, which induces cell transformation and tumor growth [53]. As expected, down-regulated genes in sorted CD133− S496 GBM daughter cells are mostly growth regulators and tumor suppressor genes (Table 2). Indeed, 11 GO clusters that are mostly related to membrane-associated components were determined (Fig. 4A, c), and 9 (30%) and 8 (27%) genes were respectively found for GO term related to "protein complex" (P value = 0.013675) and "plasma membrane" (P = 0.020780) (supplementary Table 5). This data thus suggest when CD133+ S496 GBM cells undergo cell division and produce fast-growing CD133− S496 daughter cells primarily through intrinsic cell-cycle-based mechanism. The distinctive properties between D431 and S496 GBM cells also identified through the 2-way unsupervised gene and sample clustering of non-sorted CD133+ D431 and CD133+ S496 GBM sphere cultures, which nicely segregated two groups of samples (supplementary Fig. 2; supplementary Table 6). YKL-40 was identified as the top gene overexpressed in CD133+ D431 GBM spheres (101-fold increase) when compared to CD133+ S496 GBM spheres. By contrast, transmembrane protein 47, a gene that expressed high level transcripts in brain, was identified as the top gene overexpressed in CD133+ S496 GBM sphere cultures (233-fold increase). Correspondingly, gene function enrichment analysis showed distinct molecular pathways in the growth of two different CD133+ GBM sphere lines (mesenchymal developmental pathway versus neural developmental pathway) (supplementary Fig. 2). Uniquely, four gene clusters overexpressed in CD133+ S496 spheres were found for GO terms related to cell migration, cell adhesion, cell motility, and locomotion (supplementary Fig. 2), possibly explaining the enhanced infiltrating nature of S496 tumor in mouse brain compared to that of D431 tumor (Fig. 3D).

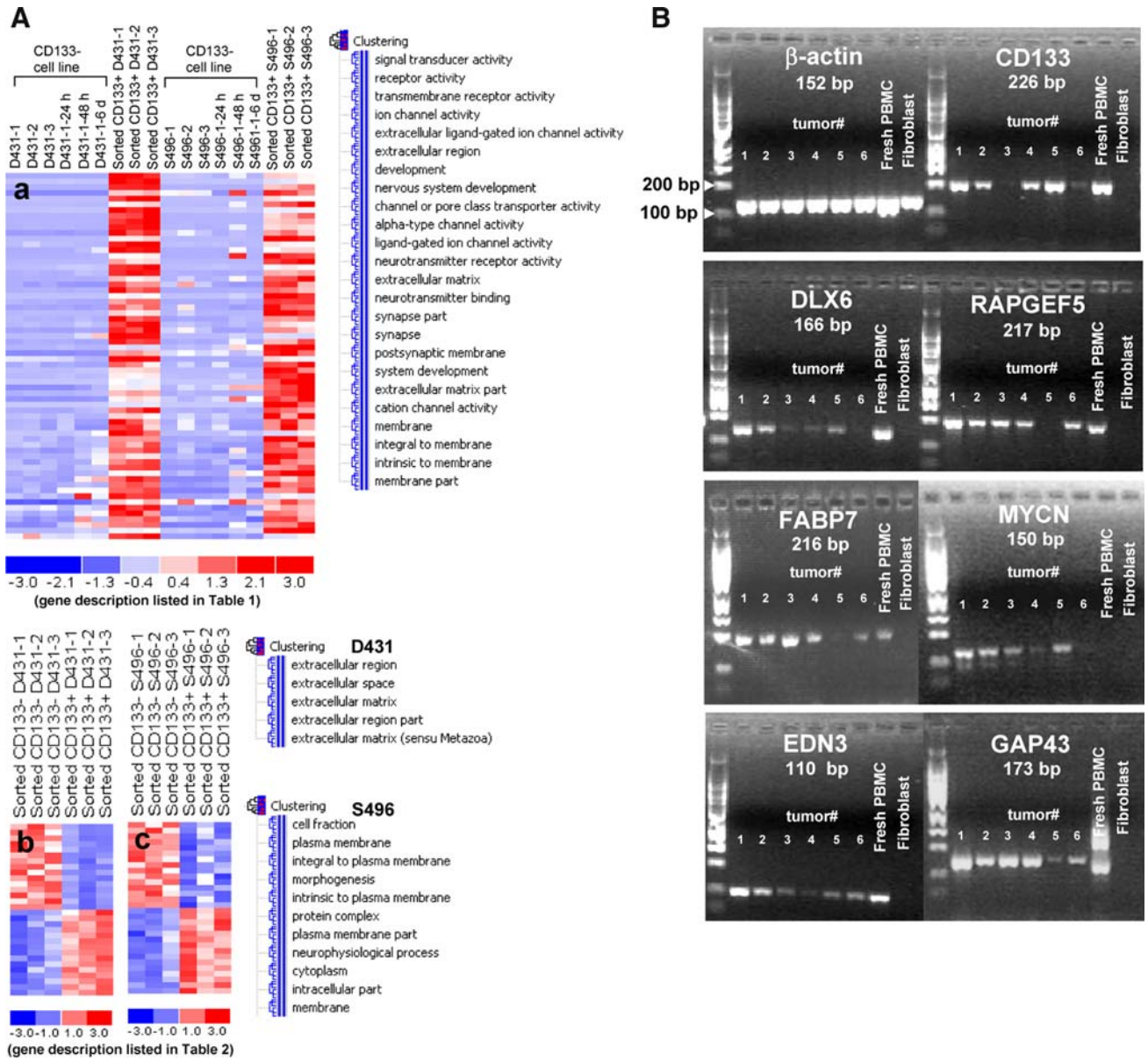

Fig. 4 Analyses of gene expression profiles of purified, tumorigenic CD133+ GBM cells sorted from the CD133+ GBM sphere cultures. **A** All plots show normalized gene expression values converted into a heat map. The log2 of the fold difference is indicated by the heat map scale at the bottom. Each column is an individual sample organized into cell types and culture conditions defined at the top. Each row is a single probe set measurement of transcript abundance for an individual gene. The genes are listed in the same order from top to bottom as the corresponding tables for each of the lists. (*a*) All genes were filtered to select transcripts with ≥3-fold expression in the tumorigenic CD133+ GBM cells (D431 and S496) sorted from the CD133+ sphere cultures (passage (p) 20, p29, and p40) compared with the non-tumorigenic, autologous CD133− GBM cells cultured in serum-containing media (p5, p10 and p15) with or without switching to a short-term NSC culture condition for 24 h, 48 h and 6 days. Sixty-four shared genes were identified from the intersection of the comparisons between CD133+ D431 GBM cells and CD133− D431 cells, and the comparison between CD133+ S496 GBM cells and CD133− S496 GBM cells. Functional categories of gene clusters upregulated in the CD133+ GBM cells were analyzed using a gene ontology annotation–based gene function enrichment analysis (d-chip software). (*b*, *c*) Gene changes in CD133− GBM daughter cells compared to CD133+ GBM daughter cells sorted from same CD133+ GBM sphere cultures. Genes that were upregulated or down-regulated with ≥1.5-fold expression in CD133− GBM daughter cells compared with CD133+ GBM daughter cells were collected. The CD133+ and CD133− GBM cells were sorted from the sphere cultures at p20, p29, and p40. Functional categories of gene clusters in GO terms were shown. **B** RT-PCR analysis showed that CD133+ GBM stem cell-associated transcripts are expressed in patient-derived GBM tumors

Table 2 Top 15 gene changes in CD133− GBM daughter cells compared to CD133+ GBM daughter cells sorted from the same CD133+ GBM sphere cultures

Gene	Symbol	Gene I.D.	Fold change	*P* value	Functional involvement
A. Genes upregulated in CD133− D431 GBM daughter cells					
Integrin-binding sialoprotein	3381	IBSP	10.13	0.01969	A major structural protein of the bone matrices; angiogenesis
Chitinase 3-like 1 (cartilage glycoprotein-39)	1116	CHI3L1	6.93	0.039091	Chondrogenesis, glioblastoma progression marker
Tryptophan 2,3-dioxygenase	6999	TDO2	5.62	0.00191	Enzyme involved in tryptophan catabolism
Fibronectin 1	2335	FN1	4.61	0.039285	Binds to integrins/extracellular matrix; promote tumor growth
Carbonic anhydrase XII	771	CA12	3.84	0.048487	Acidification of the extracellular milieu; a biomarker of gliomas
Hydroxysteroid (11-beta) dehydrogenase 1	3290	HSD11B1	3.75	0.013701	Catalyzes the interconversion of inactive cortisone to active cortisol
Solute carrier family 7	23428	SLC7A8	3.63	0.005935	Transport of neutral amino acids/essential amino acids
Stonin 2	85439	STON2	3.55	0.020396	A component of the endocytic machinery; regulates vesicle endocytosis
Plexin A4, A	57671	PLXNA4	3.48	0.039696	Mediates multiple semaphorin signals and regulates axon guidance
Calcium/calmodulin-dependent protein kinase II inhibitor 1	55450	CAMK2N1	3.42	0.011008	Inhibit brain CaM-kinase II activity
Anthrax toxin receptor 1	84168	ANTXR1	3.28	0.031259	Mediates cell spreading by coupling extracellular ligands to the actin
Growth differentiation factor 15	9518	GDF15	3.06	0.004578	Tissue differentiation and maintenance
Matrix metallopeptidase 14 (membrane-inserted)	4323	MMP14	3.03	0.01905	Angiogenesis, tumor invasion
Elastin microfibril interfacer 1	11117	EMILIN1	3.02	0.029463	Extracellular matrix constituent associated with elastic fibers
Tissue factor pathway inhibitor	3675	TFPI	3.02	0.000305	Regulates the coagulation pathway; dynamic conduction of blood
B. Genes downregulated in CD133− D431 GBM daughter cells					
Prominin 1/CD133	8842	PROM1	−8.19	0.004998	Membrane protuberances and cell polarity
Glutamate receptor, ionotrophic, AMPA 4	2893	GRIA4	−4.03	0.007852	Excitatory neurotransmitter receptors
v-Myc myelocytomatosis viral related oncogene	4613	MYCN	−3.91	0.006193	Embryonal tumor initiation factor
PRKC, apoptosis, WT1, regulator	5074	PAWR	−3.64	0.001191	Tumor suppressor; apoptosis induction
Ksp37 protein	83888	KSP37	−3.46	0.016226	Protein produced by CD4 and cytotoxic lymphocytes
Sidekick homolog 2 (chicken)	54549	SDK2	−3.43	0.011413	Cell adhesion protein that guides axonal terminals
Frizzled-related protein	2487	FRZB	−3.38	0.00987	Antagonizes Wnt pathway
Cytoplasmic FMR1 interacting protein 2	26999	CYFIP2	−3.37	0.002989	A direct p53 target gene; cellular apoptosis
Monooxygenase, DBH-like 1	26002	MOXD1	−3.31	0.006728	Predicted to hydroxylate a substrate in the endoplasmic reticulum
Complement factor H	3075	CFH	−3.13	0.011463	Inhibition of complement activation
Activated leukocyte cell adhesion molecule	29995	ALCAM	−3.08	0.002511	Marker of mesenchymal/colorectal cancer stem cells; growth control
LIM and cysteine-rich domains 1	214	LMCD1	−3.08	0.007018	Represses GATA6 in the maintenance of the differentiated phenotype

Table 2 continued

Gene	Symbol	Gene I.D.	Fold change	*P* value	Functional involvement
Scrapie responsive protein 1	11341	SCRG1	−2.98	0.010901	Mesenchymal chondrogenesis, growth suppression
v-Myb myeloblastosis viral oncogene homolog (avian)	4602	MYB	−2.97	0.049344	Intrinsic factor for neural progenitor cell proliferation
Cholinergic receptor, nicotinic, alpha polypeptide 3	1136	CHRNA5	−2.97	0.016751	Ligand-binding subunit of the ganglionic type nicotinic receptor
C. Genes upregulated in CD133− S496 GBM daughter cells					
3-Hydroxy-3-methylglutaryl-Coenzyme A synthase 1	3157	HMGCS1	3.09	0.020826	Cholesterologenesis
Solute carrier family 7	23428	SLC7A8	2.87	0.035311	Transport of neutral amino acids/essential amino acids
Mitochondrial ribosomal protein L30	51263	MRPL30	2.60	0.00943	Protein synthesis within the mitochondrion
mRNA turnover 4 homolog	51154	MRTO4	2.56	0.007082	mRNA turnover and ribosome assembly
CCAAT/enhancer binding protein zeta	10153	CEBPZ	2.31	0.010864	Maintains differentiated state; enhances osteoblastic differentiation
v-Rel reticuloendotheliosis viral oncogene homolog A	5970	RELA	2.25	0.007044	Cell survival, antiapoptosis
Endothelin 3	1908	EDN3	2.01	0.04014	Promotes neural crest cell and precursor proliferation
Guanine nucleotide binding protein-like 3 (nucleolar)-like	54552	GNL3L	1.89	0.022775	Processing of nucleolar preribosomal RNA
Adaptor-related protein complex 1, sigma 2 subunit	8905	AP1S2	1.89	0.03494	Protein sorting and assembly of endocytic vesicles
Protein kinase, cAMP-dependent, catalytic, beta	5567	PRKACB	1.62	0.04107	Proliferation and differentiation; c-myc target gene; tumorigenesis
SLIT-ROBO Rho GTPase activating protein 3	9901	SRGAP3	1.55	0.038237	Negatively regulates cell migration
Integrin, beta 8	3696	ITGB8	1.55	0.042396	Brain vascular morphogenesis in the developing CNS
Monoamine oxidase A	4128	MAOA	1.53	0.034433	Degrades amine neurotransmitters
Phosphoinositide-3-kinase, class 2, beta polypeptide	5287	PIK3C2B	1.53	0.034433	Proliferation, survival; intracellular vesicle transport
Baculoviral IAP repeat-containing 4	331	XIAP	1.52	0.022379	Blocks the apoptosis pathway via inhibiting caspase-3, 7, and 9
D. Genes downregulated in CD133− S496 GBM daughter cells					
Prominin 1/CD133	8842	PROM1	−11.00	0.039802	Membrane protuberances and cell polarity
Phosphorylase kinase, gamma 2 (testis)	5261	PHKG2	−5.95	0.008141	Activates glycogen phosphorylase
BH-protocadherin (brain–heart)	5099	PCDH7	−2.86	0.013744	Calcium-dependent cell–cell adhesion
Inhibin, beta A (activin A, activin AB alpha polypeptide)	3624	INHBA	−2.82	0.026005	Tooth development; tumor suppressor
Melanoma cell adhesion molecule	4162	MCAM	−2.81	0.013207	Putative adhesion molecule in neural crest cells/melanoma
Low density lipoprotein-related protein 1	4035	LRP1	−2.75	0.018718	Lipid metabolism; antigrowth, tumor suppressor
Leucine rich repeat neuronal 6C	158038	LINGO2	−2.69	0.014473	Expressed in limbic system and neocortex
AF4/FMR2 family, member 3	3899	AFF3	−2.68	0.008324	Regulation of lymphoid development
Nephronectin	255743	NPNT	−2.65	0.013665	Tumor suppressor
ADAM metallopeptidase with thrombospondin type 1 motif 1	9510	ADAMTS1	−2.60	0.017533	Antiangiogenesis

Table 2 continued

Gene	Symbol	Gene I.D.	Fold change	*P* value	Functional involvement
Forkhead box C1	2296	FOXC1	−2.59	0.022414	Arrests cells in the G0/G1 phase; tumor suppressor
AT rich interactive domain 1A (SWI-like)	8289	ARID1A	−2.56	0.029044	Differentiation-associated cell cycle arrest; tumor suppressor
Solute carrier family 4, anion exchanger, member 2	6522	SLC4A2	−2.52	0.025985	Housekeeping regulator of intracellular pH; tumor suppressor
La ribonucleoprotein domain family, member 1	23367	LARP1	−2.51	0.01622	Protects the 3′ end of nascent small RNAs from exonuclease digestion
Collagen, type IV, alpha 2	1284	COL4A2	−2.42	0.008793	Inhibits angiogenesis and tumor growth

Analysis was based on a cutoff of 1.5-fold changes in relative expression compared to CD133+ GBM daughter cells ($P < 0.05$)

Expression of CD133+ GBM-associated transcripts in patients' GBM tumors

Several CD133+ GBM-associated genes identified from the current two CD133+ GBM stem cell models have never been reported as GBM tumor-associated genes. By using RT-PCR analysis, a subset of selected CD133+ GBM-associated transcripts could be amplified in patient-derived GBM tumors ($n = 6$ patients) (Fig. 4B), suggesting the current culture strategy can preserve GBM stem cell properties.

Discussion

Cancer stem cell model and hypothesis has greatly changed the biological and clinical views of cancer [1–5, 54]. The molecular profiles of purified CD133+ GBM stem cells derived from the previously treated recurrent tumors characterized dormant-like cells and therefore support the hypothesis that quiescent nature of CD133+ GBM stem cells may underline the treatment resistant to the conventional therapy. The quiescent nature of cancer stem cells has been described in chronic myeloid leukemia (CML), where CML stem cells remain viable in a quiescent state even in the presence of growth factors and tyrosine kinase inhibitor [55, 56]. Indeed, while the genetic changes and tumorigenic potential were demonstrated in purified CD133+ GBM cells sorted from the CD133+ GBM spheres, the molecular profile characterized an antiproliferative nature of CD133+ GBM stem cells, suggesting the pathologic effects of molecular changes to be manifested primarily in a more differentiated progeny. Indeed, the molecular profiles of CD133+ GBM spheres (contain majority of CD133− daughter cells) initiated by the purified CD133+ GBM cells express "proliferative tumor markers" as that of CD133− GBM daughter cells, which distinctive to the quiescent CD133+ GBM daughter cells. Thus, the more differentiated CD133− GBM progeny should be considered as the true effector cells characterized fast-growing and highly angiogenic GBM tumors. The mechanisms and pathways underlying the spontaneous re-entry into active cell cycle from the quiescent state in cultures and in animal experiments remain to be elucidated [57]. In contrast to that fast-growing CD133− daughter cells, the predicted slow-cycling, non-inflammatory, and non-angiogenic nature of CD133+ GBM cells (based on the molecular profiles) may explain that GBM tumor can not be eradicated by the anti-cell cycle-based radiochemotherapy, anti-inflammatory drugs, or antiangiogenic agents.

A hallmark of all stem cells is the ability to simultaneously make identical copies of themselves (e.g. CD133+ GBM daughter cells) and give rise to a hierarchy of more differentiated progeny (e.g. CD133− GBM daughter cells). Indeed, CD133+ GBM cells fulfill this definition and are capable of undergoing cell division that give rise to a malignant tumor tissue. GBM spheres initiated with one single CD133+ GBM cell contain heterogeneous population that showed differences in cell size and proliferative potential. By RT-PCR analysis, we were able to amplify both Numb and Numb-like signals in CD133+ GBM cells (data not shown), suggesting CD133+ GBM cells may possess normal neuroepithelial-like properties capable of undergoing asymmetric cell divisions, thereby maintaining a tumor-suppressor-like phenotype [58]. Prominin/CD133 is selectively localized in protrusions of the apical membrane in neuroepithelial cells, and it was suggested that CD133 plays an important role in the maintenance of apical-basal polarity [59]. Therefore, loss of CD133 (or with other genes) may restrict CD133− GBM daughter cells to the symmetric mode of cell division and act like proliferative intermediate progenitor cells [60, 61]. Consequently, increasing the number of CD133+ GBM cells within the tumor would reflect a fast generation of proliferative and angiogenic CD133− daughter cells to form the bulk tumor [5, 62]. While our data indicated that

GBM tumor growth in these two study cases depends on the CD133+ GBM cells, GBM tumor growth seemed to depend on CD133− GBM tumor-initiating cells for other cases [63, 64]. The isolation of CD133+ GBM cells from CD133− GBM cell-initiating tumor was also reported [65], indicating the CD133 is not an obligated marker for GBM stem cells.

We previously showed that GBM tumor lines established from recurrent tumors possess mesenchymal differentiation potential [29]. A recent study further showed that GBM stem cells formed tumors capable of undergoing mesenchymal differentiation [64]. The expression of mesenchymal developmental genes in CD133+ GBM stem cells may therefore provide a potential explanation for the chondrogenic/mesenchymal differentiation in tumors [66] and the shifting toward the mesenchymal phenotype upon tumor recurrence [49]. Moreover, based on the molecular profiles of purified CD133+ GBM cells, we hypothesize that the cell-of-origin of GBM tumors may be the migratory neural crest-like cell or radial glial-like cell. Overexpression of radial glial cell (RGC) marker, FABP7, in CD133+ GBM cells supports the recent finding that RGC can give rise to adult subventricular zone stem cells [67]. On the other hand, although overexpression of MYCN is associated with a childhood malignant tumor of neural crest origin, it was recently found to be one of the most frequently amplified oncogenes in GBM tumors (42%) [68]. More samples should be analyzed in order to generalize these observations. Moreover, whether these molecular properties also applied in the general properties of CD133+ GBM cells derived from the non-treated tumor remain to be investigated. Gene expression profile analyses of GBM tumors by DNA microarrays support the notion that tumor development may indeed via distinct oncogenic mechanisms among the GBM subtypes [26, 27, 69, 70]. The thought of heterogeneity in the pathway of GBM tumor development is further supported by the recent finding in studies of expression profiles of GBM sphere cultures, which showed distinct molecular properties among the GBM stem cell lines [51, 63, 64]. Likewise, although CD133+ GBM cells sorted from CD133+ D431 and CD133+ S496 spheres express shared molecular properties, unsupervised gene and sample clustering segregated two GBM sphere lines by the genes that are associated with mesenchymal developmental pathway versus neural developmental pathway, thus implying the distinct cellular-origin of these two recurrent tumors.

In summary, we characterized CD133+ GBM stem cells isolated from two tumors that are recurrent and had previous treatment. Our in vitro and in vivo data suggest that the tumorigenic CD133+ GBM stem cells are maintained at dormant-like stage state but are able to spontaneously enter the proliferative cell cycle to generate highly proliferative and angiogenic CD133− GBM daughter cells (animal data). This observation implies that tumorigenesis may be initiated through asymmetric cell division of CD133+ GBM cells [71, 72]. Thus, identifying the genes and pathways that promote the CD133+ GBM cells entering proliferative cell division cycle may facilitate the development and design of more effective therapies that specifically target the tumorigenic potential of CD133+ GBM stem cells.

Acknowledgments This work was supported by American Cancer Society grant #RSG-07-109-01-CCE, National Brain Tumor Foundation, The Bradley Zankel Foundation, UCLA Jonsson Cancer Center Foundation and UCLA Human Gene Medicine Seed Grant.

References

1. Galli R, Binda E, Orfanelli U (2004) Isolation and characterization of tumorigenic, stem-like neural precursors from human glioblastoma. Cancer Res 64:7011–7021. doi:10.1158/0008-5472.CAN-04-1364
2. Hemmati HD, Nakano I, Lazareff JA et al (2003) Cancerous stem cells can arise from pediatric brain tumors. Proc Natl Acad Sci USA 100:15178–15183. doi:10.1073/pnas.2036535100
3. Singh SK, Hawkins C, Clarke ID et al (2004) Identification of human brain tumour initiating cells. Nature 432:396–401. doi:10.1038/nature03128
4. Yuan X, Curtin J, Xiong Y et al (2004) Isolation of cancer stem cells from adult glioblastoma multiforme. Oncogene 23:9392–9400. doi:10.1038/sj.onc.1208311
5. Bao S, Wu Q, McLendon RE et al (2006) Glioma stem cells promote radioresistance by preferential activation of the DNA damage response. Nature 444:756–760. doi:10.1038/nature05236
6. Loeffler M, Roeder I (2002) Tissue stem cells: definition, plasticity, heterogeneity, self-organization and models—a conceptual approach. Cells Tissues Organs 171:8–26. doi:10.1159/000057688
7. Fuchs E, Segre JA (2000) Stem cells: a new lease on life. Cell 100:143–155. doi:10.1016/S0092-8674(00)81691-8
8. Lavker RM, Sun TT (2000) Epidermal stem cells: properties, markers, and location. Proc Natl Acad Sci USA 97:13473–13475. doi:10.1073/pnas.250380097
9. Perryman SV, Sylvester KG (2006) Repair and regeneration: opportunities for carcinogenesis from tissue stem cells. J Cell Mol Med 10:292–308. doi:10.1111/j.1582-4934.2006.tb00400.x
10. Fuchs E, Tumbar T, Guasch G (2004) Socializing with the neighbors: stem cells and their niche. Cell 116:769–778. doi:10.1016/S0092-8674(04)00255-7 (Review)
11. Moore KA, Lemischka IR (2006) Stem cells and their niches. Science 311:1880–1885. doi:10.1126/science.1110542
12. Morrison SJ, Wandycz AM, Hemmati HD, Wright DE, Weissman IL (1997) Identification of a lineage of multipotent hematopoietic progenitors. Development 124:1929–1939
13. Schmidt GH, Winton DJ, Ponder BA (1988) Development of the pattern of cell renewal in the crypt-villus unit of chimaeric mouse small intestine. Development 103:785–790

14. Oshima H, Rochat A, Kedzia C (2001) Morphogenesis and renewal of hair follicles from adult multipotent stem cells. Cell 104:233–245. doi:10.1016/S0092-8674(01)00208-2
15. Jensen UB, Lowell S, Watt FM (1999) The spatial relationship between stem cells and their progeny in the basal layer of human epidermis: a new view based on the whole mount labelling and lineage analysis. Development 126:2409–2418
16. Jones PH, Watt FM (1993) Separation of human epidermal stem cells from transit amplifying cells on the basis of differences in integrin function and expression. Cell 73:713–724. doi:10.1016/0092-8674(93)90251-K
17. Hong KU, Reynolds SD, Giangreco A et al (2001) Clara cell secretory protein-expressing cells of the airway neuroepithelial body microenvironment include a label-retaining subset and are critical for epithelial renewal after progenitor cell depletion. Am J Respir Cell Mol Biol 24:671–681
18. Borthwick DW, Shahbazian M, Krantz QT et al (2001) Evidence for stem-cell niches in the tracheal epithelium. Am J Respir Cell Mol Biol 24:662–670
19. Reynolds SD, Giangreco A, Hong KU et al (2004) Airway injury in the pathophysiology of lung disease: selective depletion of airway stem and progenitor cells pools potentates lung inflammation and alveolar dysfunction. Am J Physiol Lung Cell Mol Physiol 287:L1256–L1265. doi:10.1152/ajplung.00203.2004
20. Bonnet D, Dick JE (1997) Human acute myeloid leukemia is organized as a hierarchy that originates from a primitive hematopoietic cell. Nat Med 3:730–737. doi:10.1038/nm0797-730
21. Vermeulen L, Todaro M, de Sousa Mello F et al (2008) Single-cell cloning of colon cancer stem cells reveals a multi-lineage differentiation capacity. Proc Natl Acad Sci USA 105:13427–13432. doi:10.1073/pnas.0805706105
22. Dalerba P, Cho RW, Clarke MF (2007) Cancer stem cells: models and concepts. Annu Rev Med 58:267–284. doi:10.1146/annurev.med.58.062105.204854 (Review)
23. Beachy PA, Karhadkar SS, Berman DM (2004) Tissue repair and stem cell renewal in carcinogenesis. Nature 432:324–331. doi:10.1038/nature03100
24. Zhang QB, Ji XY, Huang Q et al (2006) Differentiation profile of brain tumor stem cells: a comparative study with neural stem cells. Cell Res 16:909–915. doi:10.1038/sj.cr.7310104
25. Clarke MF, Dick JE, Dirks PB et al (2006) Cancer stem cells—perspectives on current status and future directions: AACR workshop on cancer stem cells. Cancer Res 66:9339–9344
26. Freije WA, Castro-Vargas FE, Fang Z et al (2004) Gene expression profiling of gliomas strongly predicts survival. Cancer Res 64:6503–6510. doi:10.1158/0008-5472.CAN-04-0452
27. Tso CL, Freije WA, Day A et al (2006) Distinct transcription profiles of primary and secondary glioblastoma subgroups. Cancer Res 66:159–167. doi:10.1158/0008-5472.CAN-05-0077
28. Tso CL, Shintaku P, Chen J et al (2006) Primary glioblastomas express mesenchymal stem-like properties. Mol Cancer Res 4:607–619. doi:10.1158/1541-7786.MCR-06-0005
29. Guan Y, Gerhard B, Hogge DE (2003) Detection, isolation, and stimulation of quiescent primitive leukemic progenitor cells from patients with acute myeloid leukemia (AML). Blood 101:3142–3149. doi:10.1182/blood-2002-10-3062
30. Bez A, Corsini E, Curti D et al (2003) Neurosphere and neurosphere-forming cells: morphological and ultrastructural characterization. Brain Res 993:18–29. doi:10.1016/j.brainres.2003.08.061
31. Flanagan LA, Rebaza LM, Derzic S et al (2006) Regulation of human neural precursor cells by laminin and integrins. J Neurosci Res 83:845–856. doi:10.1002/jnr.20778
32. Jacques TS, Relvas JB, Nishimura S et al (1998) Neural precursor cell chain migration and division are regulated through different beta1 integrins. Development 125:3167–3177
33. Hsu SH, Noamani B, Abernethy DE et al (2006) Dlx5- and Dlx6-mediated chondrogenesis: differential domain requirements for a conserved function. Mech Dev 123:819–830. doi:10.1016/j.mod.2006.08.005
34. Weston AD, Rosen V, Chandraratna RA et al (2000) Regulation of skeletal progenitor differentiation by the BMP and retinoid signaling pathways. J Cell Biol 148:679–690. doi:10.1083/jcb.148.4.679
35. Enomoto-Iwamoto M, Kitagaki J, Koyama E et al (2002) The Wnt antagonist Frzb-1 regulates chondrocyte maturation and long bone development during limb skeletogenesis. Dev Biol 251:142–156. doi:10.1006/dbio.2002.0802
36. Barker N, van Es JH, Kuipers J et al (2007) Identification of stem cells in small intestine and colon by marker gene Lgr5. Nature 449:1003–1007. doi:10.1038/nature06196
37. Chen Y, Leal AD, Patel S (2007) The homeobox gene GAX activates p21WAF1/CIP1 expression in vascular endothelial cells through direct interaction with upstream AT-rich sequences. J Biol Chem 282:507–517. doi:10.1074/jbc.M606604200
38. Narita K, Staub J, Chien J et al (2006) HSulf-1 inhibits angiogenesis and tumorigenesis in vivo. Cancer Res 66:6025–6032. doi:10.1158/0008-5472.CAN-05-3582
39. Kovalenko D, Yang X, Nadeau RJ et al (2003) Sef inhibits fibroblast growth factor signaling by inhibiting FGFR1 tyrosine phosphorylation and subsequent ERK activation. J Biol Chem 278:14087–14091. doi:10.1074/jbc.C200606200
40. Chen Y, Hu Y, Lu K et al (2007) Very low density lipoprotein receptor, a negative regulator of the wnt signaling pathway and choroidal neovascularization. J Biol Chem 282:34420–34428. doi:10.1074/jbc.M611289200
41. Lahav R, Dupin E, Lecoin L (1998) Endothelin 3 selectively promotes survival and proliferation of neural crest-derived glial and melanocytic precursors in vitro. Proc Natl Acad Sci USA 95:14214–14219. doi:10.1073/pnas.95.24.14214
42. Shen Y, Mani S, Meiri KF (2004) Failure to express GAP-43 leads to disruption of a multipotent precursor and inhibits astrocyte differentiation. Mol Cell Neurosci 26:390–405. doi:10.1016/j.mcn.2004.03.004
43. Mita R, Coles JE, Glubrecht DD et al (2007) B-FABP-expressing radial glial cells: the malignant glioma cell of origin? Neoplasia 9:734–744. doi:10.1593/neo.07439
44. Kaloshi G, Mokhtari K, Carpentier C et al (2007) FABP7 expression in glioblastomas: relation to prognosis, invasion and EGFR status. J Neurooncol 84:245–248. doi:10.1007/s11060-007-9377-4
45. Biernat W, Kleihues P, Yonekawa Y et al (1997) Amplification and overexpression of MDM2 in primary (de novo) glioblastomas. J Neuropathol Exp Neurol 56:180–185. doi:10.1097/00005072-199702000-00009
46. Edenfeld G, Altenhein B, Zierau A et al (2007) Notch and Numb are required for normal migration of peripheral glia in Drosophila. Dev Biol 301:27–37. doi:10.1016/j.ydbio.2006.11.013
47. Sakamoto M, Hirata H, Ohtsuka T et al (2003) The basic helix-loop-helix genes Hesr1/Hey1 and Hesr2/Hey2 regulate maintenance of neural precursor cells in the brain. J Biol Chem 278:44808–44815. doi:10.1074/jbc.M300448200
48. Deneen B, Ho R, Lukaszewicz A et al (2006) The transcription factor NFIA controls the onset of gliogenesis in the developing spinal cord. Neuron 52:953–968. doi:10.1016/j.neuron.2006.11.019
49. Jeon HM, Jin X, Lee JS et al (2008) Inhibitor of differentiation 4 drives brain tumor-initiating cell genesis through cyclin E and notch signaling. Genes Dev 22:2028–2033. doi:10.1101/gad.1668708
50. Anthony TE, Mason HA, Gridley T et al (2005) Brain lipid-binding protein is a direct target of Notch signaling in radial glial cells. Genes Dev 19:1028–1033. doi:10.1101/gad.1302105

51. Phillips HS, Kharbanda S, Chen R et al (2006) Molecular subclasses of high-grade glioma predict prognosis, delineate a pattern of disease progression, and resemble stages in neurogenesis. Cancer Cell 9:157–173. doi:10.1016/j.ccr.2006.02.019
52. Coleman PS (1986) Membrane cholesterol and tumor bioenergetics. Ann N Y Acad Sci 488:451–467. doi:10.1111/j.1749-6632.1986.tb46578.x
53. Wu KJ, Mattioli M, Morse HC et al (2002) c-MYC activates protein kinase A (PKA) by direct transcriptional activation of the PKA catalytic subunit beta (PKA-Cbeta) gene. Oncogene 21: 7872–7882. doi:10.1038/sj.onc.1205986
54. Al-Hajj M, Becker MW, Wicha M et al (2004) Therapeutic implications of cancer stem cells. Curr Opin Genet Dev 14:43–47. doi:10.1016/j.gde.2003.11.007 (Review)
55. Holyoake T, Jiang X, Eaves C, Eaves A (1999) Isolation of a highly quiescent subpopulation of primitive leukemic cells in chronic myeloid leukemia. Blood 94:2056–2064
56. Graham SM, Jørgensen HG, Allan E et al (2002) Primitive, quiescent, Philadelphia-positive stem cells from patients with chronic myeloid leukemia are insensitive to STI571 in vitro. Blood 99:319–325. doi:10.1182/blood.V99.1.319
57. Sang L, Coller HA, Roberts JM (2008) Control of the reversibility of cellular quiescence by the transcriptional repressor HES1. Science 321:1095–1100. doi:10.1126/science.1155998
58. Chia W, Somers WG, Wang H (2008) Drosophila neuroblast asymmetric divisions: cell cycle regulators, asymmetric protein localization, and tumorigenesis. J Cell Biol 180:267–272. doi: 10.1083/jcb.200708159
59. Kosodo Y, Roper K, Haubensak W et al (2004) Asymmetric distribution of the apical plasma membrane during neurogenic divisions of mammalian neuroepithelial cells. EMBO J 23:2314–2324. doi:10.1038/sj.emboj.7600223
60. Pontious A, Kowalczyk T, Englund C et al (2008) Role of intermediate progenitor cells in cerebral cortex development. Dev Neurosci 30:24–32. doi:10.1159/000109848
61. Bello BC, Izergina N, Caussinus E et al (2008) Amplification of neural stem cell proliferation by intermediate progenitor cells in Drosophila brain development. Neural Dev 3:5. doi:10.1186/1749-8104-3-5
62. Zeppernick F, Ahmadi R, Campos B et al (2008) Stem cell marker CD133 affects clinical outcome in glioma patients. Clin Cancer Res 14:123–129. doi:10.1158/1078-0432.CCR-07-0932
63. Gunther HS, Schmidt NO, Phillips HS et al (2008) Glioblastoma-derived stem cell-enriched cultures form distinct subgroups according to molecular and phenotypic criteria. Oncogene 27: 2897–2909. doi:10.1038/sj.onc.1210949
64. Beier D, Hau P, Proescholdt M et al (2007) CD133(+) and CD133(−) glioblastoma-derived cancer stem cells show differential growth characteristics and molecular profiles. Cancer Res 67:4010–4015. doi:10.1158/0008-5472.CAN-06-4180
65. Wang J, Sakariassen PØ, Tsinkalovsky O et al (2008) CD133 negative glioma cells form tumors in nude rats and give rise to CD133 positive cells. Int J Cancer 122:761–768. doi:10.1002/ijc.23130
66. Ricci-Vitiani L, Pallini R, Larocca LM et al (2008) Mesenchymal differentiation of glioblastoma stem cells. Cell Death Differ 15:1491–1498. doi:10.1038/cdd.2008.72
67. Merkle FT, Tramontin AD, Garcia-Verdugo JM et al (2004) Radial glia give rise to adult neural stem cells in the subventricular zone. Proc Natl Acad Sci USA 101:17528–17532. doi: 10.1073/pnas.0407893101
68. Hui AB, Lo KW, Yin XL et al (2001) Detection of multiple gene amplifications in glioblastoma multiforme using array-based comparative genomic hybridization. Lab Invest 81:717–723
69. Nutt CL, Mani DR, Betensky RA et al (2003) Gene expression-based classification of malignant gliomas correlates better with survival than histological classification. Cancer Res 63:1602–1607
70. Ohgaki H, Kleihues P (2007) Genetic pathways to primary and secondary glioblastoma. Am J Pathol 170(5):1445–1453. doi: 10.2353/ajpath.2007.070011 Review
71. Lee M, Vasioukhin V (2008) Cell polarity and cancer-cell and tissue polarity as a non-canonical tumor suppressor. J Cell Sci 121: 1141–1150. doi:10.1242/jcs.016634
72. Wodarz A, Nathke I (2007) Cell polarity in development and cancer. Nat Cell Biol 9:1016–1024. doi:10.1038/ncb433